

1  
2  
3  
4 **An experimental investigation of the explosion characteristics of**  
5 **dimethyl ether-air mixtures**  
6  
7

8 Bo Zhang<sup>1,2†</sup>, Hoi Dick Ng<sup>3</sup>  
9  
10

11  
12  
13  
14  
15 <sup>1</sup> East China University of Science and Technology  
16 State Environmental Protection Key Laboratory of Environmental Risk Assessment and Control  
17 on Chemical Process, Shanghai, 200237, China  
18

19 <sup>2</sup> Beijing Institute of Technology  
20 State Key Laboratory of Explosion Science and Technology, Beijing, 100081, China  
21

22 <sup>3</sup> Concordia University  
23 Department of Mechanical and Industrial Engineering  
24 Montréal, QC, H3G 1M8, Canada  
25

26 †Corresponding Author  
27

28 E-mail: bzhang@ecust.edu.cn  
29

30 Tel.: (86) 21-64253132  
31 Fax: (86) 21-64253404  
32

# An experimental investigation of the explosion characteristics of dimethyl ether-air mixtures

## Abstract

In this work, experiments are performed to study the explosion characteristics of dimethyl ether (DME) -air mixtures using a standard 20-L spherical explosion test apparatus. The experimental data reported in this paper includes: the maximum explosion pressure ( $p_{\max}$ ), flammability limits, maximum rate of pressure rise  $(dp/dt)_{\max}$ , and combustion properties (i.e., laminar burning velocity, flame radius) of DME-air mixtures at different initial conditions. The experimental results indicate that the variation between  $p_{\max}$  and DME concentration ( $C_{\text{DME}}$ ) exhibits a typical inverse “U” shaped behavior, with the peak  $p_{\max}$  at slightly larger than the stoichiometric concentration.  $p_{\max}$  is also found to decrease as the initial pressure goes down. As the initial pressure decreases from 100 kPa to 40 kPa, the lower flammability limit (LFL) is observed to vary slightly, while the upper flammability limit (UFL) is found to have a more significant drop. The relation between  $(dp/dt)_{\max}$  and  $C_{\text{DME}}$  behaves similarly as that of  $p_{\max}$  as a function of  $C_{\text{DME}}$ , and the explosion pressure rises more abruptly at higher initial pressure. A satisfactory agreement is also found between the laminar burning velocity determined experimentally from the pressure measurement and that computed by PREMIX simulations. The present experimental results also show that the increase of the dimensionless radius of the flame is slower at higher initial pressure.

**Keywords:** Dimethyl ether; Maximum explosion pressure; Flammability limits; Maximum rate of pressure rise; Laminar burning velocity; Flame radius.

## 57 **1 Introduction**

58 Dimethyl ether (DME:CH<sub>3</sub>OCH<sub>3</sub>) is a promising oxygenated fuel that has the potential to be  
59 used as an alternative to natural gas for power production and as a substitute for diesel fuel.  
60 DME has high oxygen content of 35 % by weight, making the combustion smokeless and a high  
61 tolerance to exhaust gas recirculation [1]. The use of DME has been proven to significant  
62 decrease particulate formation, nitrogen or sulfur oxides (NO<sub>x</sub> and SO<sub>x</sub>), and carbon monoxide  
63 (CO) emission [2, 3]. DME also has a high Cetane number of 55 to 60 and a boiling point of  
64 -25 °C. These properties are ideal for fast mixture formation, reduction in ignition delay, and  
65 cold start for diesel engines [4].

66 Due to its potential as a future alternative fuel, the combustion characteristics of DME have  
67 attracted significant attention in recent years [5-10]. A number of experimental and numerical  
68 studies can be found in the literature on the combustion and emission characteristics of DME  
69 under engine conditions [11-13]. Fundamental properties such as flammability and laminar  
70 burning velocities [14-17], and combustion processes of DME under turbulent conditions [3]  
71 were also reported. Detailed chemical mechanisms for low and high temperature DME oxidation  
72 have been developed and validated [18, 19], and a recent mechanism for DME mixture at high  
73 pressures was also constructed by Burke et al. [20]. Furthermore, the effects of DME addition  
74 on the high-temperature ignition and burning properties of methane-air mixtures were studied  
75 experimentally and numerically [21]. Premixed and non-premixed ignition of methane/DME  
76 binary fuel blends with hot air has been investigated through numerical simulation with detailed  
77 chemistry and complete thermo-chemical as well as transport properties [22]. Detonation  
78 velocities and characteristic cell sizes of DME-oxygen and DME-air mixtures have been  
79 measured by Ng et al. [23] and Diakow et al. [24], and the explosion and detonation

80 characteristics of DME were experimentally investigated using a 180-L spherical vessel and a  
81 large-scale detonation tube by Mogi and Horiguchi [25]. In addition, experiments were also  
82 carried out to examine the leakage and explosion of liquid DME [26].

83 While DME flames have been studied extensively, comparatively little information exists  
84 on the explosion characteristics, e.g., flammability limits, maximum explosion pressure,  $p_{\max}$ ,  
85 maximum rate of pressure rise,  $(dp/dt)_{\max}$  of DME at various initial conditions. The knowledge  
86 of the explosion characteristics of DME is of importance to ensure the safety in industries that  
87 produce or use it. A realistic assessment of the explosion hazards of DME is necessary for  
88 preventive measures of explosion accidents and the design of effective mitigation schemes.  
89 Among those aforementioned combustion and explosion characteristics, a key combustion  
90 property is the laminar burning velocity ( $S_L$ ) which is the velocity of a steady one-dimensional  
91 adiabatic free flame propagating in the doubly infinite domain [27]. It received particular  
92 attention not only because it represents a basic characteristic property (e.g., reactivity, diffusivity,  
93 and exothermicity) of the premixed combustible gasses [28], its accurate knowledge is also  
94 essential for engine design, modeling of turbulent combustion, and validation of chemical  
95 kinetic mechanisms. In addition, the determination of laminar burning velocity is very important  
96 for the analysis and calculations used in the field of explosion protection [29]. Besides  
97 experimental measurement, the laminar burning velocity can also be estimated by numerical  
98 calculation through PREMIX simulations [30], or by semi-empirical mathematical model [31,  
99 32]. The results obtained from experimental measurement and numerical calculation can then be  
100 compared for validation and assessment, together with data reported in the literature [4, 33].

101 The objective of the present study was twofold. First, the explosion parameters of DME-air  
102 mixtures are systematically measured from experiment. The explosion parameters include: the

103 maximum explosion pressure  $p_{\max}$ , both lower flammability limit (LFL) and upper flammability  
104 limit (UFL), and the maximum rate of pressure rise  $(dp/dt)_{\max}$ . Second, the combustion  
105 characteristics (i.e., laminar burning velocity and the evolution of flame radius) are examined in  
106 detail under different initial conditions. The laminar burning velocity obtained from different  
107 methods are also compared and discussed.

108

## 109 **2 Experimental details**

### 110 **2.1 Experimental setup**

111 Measurements of the explosion parameters in DME-air mixtures were carried out in a standard  
112 20-L explosion spherical vessel conforming to the international standard ISO6184-1, see Fig. 1.  
113 It essentially consists of an explosion chamber, an electric ignition system, a control unit, a data  
114 acquisition system, a release valve, a vacuum pump and an air compressor. High-voltage electric  
115 spark was used to supply ignition energy as in previous studies [34-39]. The igniter was  
116 mounted at the center of the spherical bomb and a spark energy of 10 J, estimated from  $1/2 CU^2$   
117 (“ $C$ ” and “ $U$ ” refer the capacitance and voltage, respectively.  $C = 0.1102 \times 10^{-3}$  F,  $U = 426$  V),  
118 was delivered by an electric ignition system.

119

### 120 **2.2 Experimental procedure and conditions**

121 For the explosion experiments, gas concentrations were regulated by the gas partial pressures.  
122 The purity of the DME used in this experiment is 99.8 %. During the experiments, the explosion  
123 pressure evolutions were measured by a PCB pressure transducer installed in the vessel wall and  
124 recorded by a data acquisition system for each shot. These data yielded values of the maximum  
125 explosion pressure and maximum rate of pressure rise as illustrated in Fig. 2. This figure shows

126 a typical pressure history of the DME-air of  $C_{\text{DME}} = 10\%$  at an initial pressure  $p_0$  of 100 kPa.  
127 The combustion time  $t_c$  is defined as the period from ignition to the time when the overpressure  
128 reaches its maximum. The measurements were repeated at least 3 times, and results were  
129 presented in the figures with error bars determined by the standard deviation. The main sources  
130 of the small variation can stem from the effect of wall cooling, ignition source, the degree of  
131 mixture homogeneity and asymmetry [40]. In this study, a wide range of initial conditions of  
132 DME-air mixtures were used. The initial pressure ranges from 40 kPa to 100 kPa, and fuel  
133 concentrations are from 3 to 19.5 %.

### 134 **3 Results and discussion**

#### 135 **3.1 Maximum explosion pressure**

136 Gas explosion max-overpressure is an important parameter of evaluating the explosion hazard. It  
137 reflects the energy distribution of explosive waves in their propagation process [41-46]. The  
138 measurement of the explosion pressure in quiescent DME-air mixtures with various  
139 compositions at the ambient condition are summarized in Table 1. In this table,  $p_{\text{max}}$  and its  
140 corresponding  $t_c$  are directly obtained from the pressure history. For comparison, the adiabatic  
141 pressure  $p_{\text{ad}}$  is also given and is calculated from thermo-chemical analysis using the GASEQ  
142 software [47]. These experimental data of  $p_{\text{max}}$  are also compared with those reported by Mogi  
143 and Horiguchi [25], and a curve fit of  $p_{\text{max}}$  using smoothing splines is also given for better  
144 comparison, see Fig. 3. The explosion pressure reaches its maximum value at a composition of  
145 7.5 %, which is slightly larger than the stoichiometric concentration (6.5 %). A similar behavior  
146 is also observed by Mogi and Horiguchi [25] in their 180-L spherical vessel. Near the  
147 stoichiometric condition, both the present data as well as the results by Mogi and Horiguchi [25]  
148 agree well with the adiabatic explosion pressure determined from chemical equilibrium within

149 the experimental uncertainties. The experimental measurement starts to deviate from the  
150 adiabatic pressure at off-stoichiometric conditions, prominently on the rich side. As pointed out  
151 by Mogi and Horiguchi [25], at those conditions the combustion speed decreases and the event  
152 departs from its constant-volume explosion character. Incomplete combustion and the effect of  
153 cooling also give rise to this discrepancy, which are susceptible to the scale of the apparatus. In  
154 fact, it can also be seen from Fig. 3 that, the results of  $p_{\max}$  from this study are slightly larger  
155 than those of Mogi and Horiguchi near stoichiometric concentration, though within  
156 experimental uncertainties. A contrary behavior is also observed as the composition tends to  
157 both the fuel lean and rich sides. It is noteworthy that in [25], Mogi and Horiguchi used a 180-L  
158 spherical vessel, while the present study is performed using a 20-L one. Thus, the discrepancy at  
159 off-stoichiometric conditions can be caused by the wall cooling effects. Near stoichiometric  
160 conditions, the combustion speed is high and the cooling rate has less influence on the  
161 overpressure. However, for incomplete combustion where the temperature is lower (i.e., at off  
162 stoichiometric conditions), the combustion speed becomes slower, which allows a longer time  
163 scale of the phenomenon for the cooling effect to come into play. The faster cooling of a smaller  
164 volume in the 20-L chamber, as compared to the 180-L large-scale apparatus used by Mogi and  
165 Horiguchi [25], thus results in a lower overpressure.

166        Figures 4 to 6 show the results of  $p_{\max}$  for different DME compositions at an initial pressure  
167 lower than the atmospheric condition, i.e., 80 kPa, 60 kPa and 40 kPa. To show the general trend  
168 in the experimental data, curve fits using a third order polynomial are also plotted for better  
169 visualization. Note that there is no previous experimental data at those pressure values for direct  
170 comparison. Therefore, the measured data are merely compared with the chemical equilibrium  
171 results obtained using the GASEQ software [47]. Similarly, large difference is observed as the

172 condition moves toward the LFL and UFL. Again, the theoretical maximum explosion pressure  
173 determined from the equilibrium calculation is based on the hypothesis of ideal adiabatic  
174 explosion. As the composition tends to fuel-lean or fuel-rich sides, not only incomplete reaction  
175 occurs but also the heat loss to the surrounding can affect the explosion process, making the  
176 measured values different from the chemical equilibrium calculation of an ideal adiabatic  
177 explosion. It is observed from Figs. 4 to 6 that the value of  $p_{\max}$  goes down as the initial pressure  
178 decreases. This observation perhaps suggests that the faster reactivity induced by the higher  
179 initial pressure reduces the effect of heat losses on the explosion process. Hence, the higher  
180 initial pressure may maintain higher explosion temperature, which in turn results in the rise of  
181 overpressure.

182

### 183 **3.2 Flammability limits**

184 Table 2 shows the LFL and UFL for the DME-air mixture at different initial pressures. These  
185 limits were determined when half of the shots at the same condition indicate no occurrence of  
186 explosion. It is observed that the LFL has only a small fluctuation as the initial pressure  
187 decreases, i.e., only a small increase from 3.5 % to 3.75 % as the initial pressure changes from  
188 100 kPa to 40 kPa. However, the UFL is found to have relatively a more significant drop, which  
189 changes from 19 % to 12.5 %. Reducing the initial pressure is found to narrow the interval width  
190 of these two limits. It is worth to point out that this observed behavior is similar to hydrogen/air  
191 [48] in which the lower flammability limit is not significantly sensitive to the initial pressure,  
192 while the latter has more significant effect on the UFL. From the chemical kinetic point-of-view,  
193 the effect of pressure increase has an influence on the reaction rates, especially those involved  
194 third body collisions. As shown in [33], reaction steps involving H and methyl radicals show

195 greater sensitivity for rich mixtures at high pressure. Such kinetic effect may thus render the  
196 UFL more sensitive to the initiate pressure.

197

### 198 **3.3 Maximum rate of pressure rise**

199 The maximum rate of pressure rise  $(dp/dt)_{\max}$  is a commonly examined parameter for explosion  
200 characteristics evaluation and used in deflagration index determination as in several previous  
201 studies [49, 50]. The results of  $(dp/dt)_{\max}$  as a function of DME concentration at different initial  
202 pressures are shown in Fig. 7. It can be seen that, the relation between  $(dp/dt)_{\max}$  and  $C_{\text{DME}}$  is  
203 very similar as that of  $p_{\max}$  as a function of  $C_{\text{DME}}$ . The result indicates that the pressure rises  
204 more abruptly at higher initial pressure. While for the same initial pressure, the value of  
205  $(dp/dt)_{\max}$  is larger near the stoichiometric condition.

206 It is noteworthy that the rate of pressure rise reaches its maximum value at a slightly higher  
207 concentration of approximately 7.5 % ( $\varphi = 1.159$ ) than the stoichiometric condition ( $\varphi = 1$ ), with  
208 a mean value of 46.09 MPa/s. Although this behavior is similar to that for the natural gas  
209 (NG)-air mixture observed in Zhang et al. [29] (with an average value of 18.86 MPa/s at the NG  
210 concentration of 10.5 % or  $\varphi = 1.117$ ), yet the pressure increases more abruptly in DME-air than  
211 in NG-air mixtures.

212

### 213 **3.4 Laminar burning velocity**

214 Laminar burning velocity ( $S_L$ ) is a unique property of a combustible mixture, indicating its  
215 reactivity and exothermicity in a given diffusive medium. Since it contains the physico-chemical  
216 information of the mixture, many premixed flame phenomena, e.g., extinction, flash back,  
217 blow-off, and turbulent flame propagation, can be characterized with  $S_L$  being a reference

218 parameter [28]. In this study, the laminar burning velocity is computed through two different  
 219 methods. The first one uses the PREMIX module of the CHEMKIN-II. The PREMIX code  
 220 adopts a hybrid time-integration/Newton-iteration technique to solve the steady-state mass,  
 221 species and energy conservation equations for a freely propagating flame. It has been widely  
 222 used in many previous studies [21, 51-54]. In this study, 1200 grid points are imposed in the  
 223 PREMIX calculations to assure a fully converged prediction. Also a small time-step  $\Delta t =$   
 224  $5.0 \times 10^{-7}$  sec is used for the computation. The present PREMIX calculation is coupled with the  
 225 reaction scheme [14] involving 46 species and 263 reactions. This reaction mechanism was also  
 226 used previously by Chen et al. [21] to perform PREMIX calculations of the laminar burning  
 227 velocities for DME/CH<sub>4</sub>/air mixtures. The mechanism was verified by Chen et al. [21] by  
 228 comparing measured laminar burning velocities from experiment with calculations and the result  
 229 shows reasonable agreement with the largest difference less than 10 %. The second method  
 230 considers a mathematical model proposed by Dahoe et al. [31, 32], in which the laminar burning  
 231 velocity depends on  $p_{\max}$  and  $dp/dt$ .  $S_L$  calculated by this model was also used in our previous  
 232 study of NG-air mixtures [29]. The model gives the following expression:

$$233 \quad S_L = \frac{1}{(p_{\max} - p_0)} \frac{1}{3} \left( \frac{4\pi}{3V} \right)^{-1/3} \left( \frac{p_0}{p} \right)^{1/\gamma} \left[ 1 - \left( \frac{p_0}{p} \right)^{1/\gamma} \times \left( \frac{p_{\max} - p}{p_{\max} - p_0} \right) \right]^{-2/3} \frac{dp}{dt} \quad (1)$$

234 where  $V$  is the vessel volume,  $p$  and  $p_0$  are the actual pressure and initial pressure,  $\gamma$  the adiabatic  
 235 coefficient of the unburned gas.  $S_L$  is determined by a fitting method proposed by Dahoe, in  
 236 which  $S_L$  is calculated by fitting the pressure history measurement (i.e., actual pressure  $p$  and  
 237  $dp/dt$ ). A pressure ( $p$ )- laminar burning velocity ( $S_L$ ) curve is then obtained. Afterwards,  $S_{L0}$  at  
 238 the reference pressure (i.e., 100 kPa) can be determined by the extrapolate data from a linear  
 239 curve fit of  $p$ - $S_L$ . [55-57].  $S_L$  is calculated at a flame radius greater than 6 mm to avoid the effect

240 associated to the spark ignition [58], so the result can be considered as an ideal spherical flame  
241 propagating outward.

242 The laminar burning velocity of DME-air mixtures at different equivalence ratios under 100  
243 kPa determined using the two aforementioned techniques are shown in Fig. 8. The reported  
244 results by Qin and Ju [33] and Daly et al. [4] are also included in the same figure for comparison.  
245 As shown in Fig. 8, it appears that the computed laminar burning velocity from Eq. (1) agrees  
246 reasonably well with the PREMIX simulation. The largest difference between these two sets of  
247 data is 42.93 % at the fuel rich condition at 100 kPa. At this condition however, the results from  
248 Eq. (1) are very close to the experimental data reported by Qin and Ju [33]. Overall, one can  
249 argue that the above comparison shows no significant difference for computing the laminar  
250 burning velocity using Eq. (1) and the PREMIX code. Similar comparisons of the computed  
251 laminar burning velocity of DME-air mixtures at different equivalence ratios with initial  
252 pressures of 80 kPa, 60 kPa and 40 kPa are also shown in Fig. 9. Again, a reasonable agreement  
253 between the two results still holds.

254 Figures 8 and 9 also indicate a decreasing trend of  $S_L$  with the increase of initial pressure,  
255 e.g.,  $S_L$  is found to be 61.52 cm/s at 40 kPa which is larger than 48.40 cm/s at 100 kPa at the  
256 same composition of  $C_{DME} = 7.5\%$ . The behavior of decreasing trend of  $S_L$  with the increase of  
257 initial pressure is caused by the increasing density,  $\rho_u$ , with increasing pressure. As demonstrated  
258 by Law [28], the eigenvalue for flame propagation is  $S_L = f^0/\rho_u$ , (where  $f^0$  and  $\rho_u$  are the mean  
259 laminar burning flux and density, respectively). By increasing pressure,  $f^0$  increases. It  
260 demonstrates that the increase in density with pressure dominates over the retarding effect of  $S_L$ .

261

### 262 3.5 Flame radius

263 The flame radius,  $r_f$ , is also calculated through the equation proposed by Dahoe et al. [31, 32] as  
264 follows:

$$265 \quad r_f = \left( \frac{3V}{4\pi} \right)^{1/3} \left[ 1 - \left( \frac{p_0}{p} \right)^{1/\gamma} \left( \frac{p_{\max} - p}{p_{\max} - p_0} \right) \right]^{1/3} \quad (2)$$

$$266 \quad \bar{r} = r_f / r_a \quad (3)$$

267 where  $r_f$  is the flame radius,  $r_a$  the radius of the vessel and  $\bar{r}$  the dimensionless radius of burned  
268 gas. The typical results for stoichiometric DME-air mixtures at different initial pressures are  
269 shown in Fig. 10. It can be seen that the flame radius increases just after the time of 0.02 sec,  
270 and it increases rapidly until it reaches the wall of the spherical chamber. This process is  
271 established as the pressure rise stage. Figure 10 also shows that at the same given time, the  
272 dimensionless radius of the flame is relatively greater (i.e., the flame propagates to a longer  
273 distance at the same time) at lower initial pressure, which is due to the higher burning velocity.

274

### 275 4 Concluding remarks

276 This paper presents a detailed investigation on the explosion characteristics (i.e., maximum  
277 explosion pressure, flammability limits, maximum rate of pressure rise) and combustion  
278 properties (i.e., laminar burning velocity, flame radius) of DME-air mixtures. Experiments are  
279 performed by systematically measuring the pressure evolutions in a standard 20-L explosion  
280 spherical vessel.

281 The present measurement shows that the variation between  $p_{\max}$  and DME concentration  
282 ( $C_{\text{DME}}$ ) exhibits a typical inverse “U” shaped behavior, and  $p_{\max}$  reaches its peak value when its  
283 equivalence ratio is slightly larger than 1. It is found from the present measurement that  $p_{\max}$

284 decreases as the initial pressure goes down. The flammability region is found to be from 3.5 %  
285 to 19 % of DME by volume at the ambient condition. As the initial pressure decreases from 100  
286 kPa to 40 kPa, the LFL varies slightly and shows little sensitivity to the initial pressure, while  
287 the UFL exhibits a more significant drop. The experimental data also show that the explosion  
288 pressure rises more abruptly at higher initial pressure. The relation between  $(dp/dt)_{\max}$  and  $C_{\text{DME}}$   
289 is found to be very similar to that of  $p_{\max}$  as a function of  $C_{\text{DME}}$ . Laminar burning velocity was  
290 also estimated using both the PREMIX simulation and a mathematical model based on the  
291 measured pressure evolution, and a satisfactory agreement is found between those results,  
292 especially for  $C_{\text{DME}} \leq 9.5\%$ . A decreasing trend of  $S_L$  is observed with the increase of initial  
293 pressure. This is due to the resulting increase in density with pressure causing the decreasing the  
294 observed retarding effect of  $S_L$ . Finally, the calculated dimensionless radius of the flame from  
295 the pressure history is found to be smaller at higher initial pressure.

296

## 297 **Acknowledgments**

298 This work is supported by the National Natural Science Foundation of China (Grant No.:  
299 11402092), Fundamental Research Funds for the Central Universities (Grant No.:  
300 222201314030), and the opening project of State Key Laboratory of Explosion Science and  
301 Technology, Beijing Institute of Technology (Grant No.:KFJJ15-03M).

302

303

## **References**

- 304 [1] S. H. Park, C. S. Lee. Combustion performance and emission reduction characteristics of automotive  
305 DME engine system. Prog. Energ. Combust. 39 (2013): 147-168. DOI:10.1016/j.pecs.2012.10.002
- 306 [2] X. C. Lu, D. Han, Z. Huang. Fuel design and management for the control of advanced  
307 compression-ignition combustion modes. Prog. Energ. Combust. 37 (2011): 741-783.

308 DOI:10.1016/j.pecs.2011.03.003

309 [3] K. N. Gabet, H. Shen, R. A. Patton, F. Fuest, J. A. Sutton. A comparison of turbulent dimethyl ether  
310 and methane non-premixed flame structure. *Proc. Combust. Inst.* 34 (2013): 1447-1454.

311 DOI:10.1016/j.proci.2012.06.183

312 [4] C. A. Daly, J. M. Simmie, J. Würmel, N. Djebaili, C. Paillard. Burning velocities of dimethyl ether  
313 and air. *Combust. Flame* 125 (2001): 1329-1340. DOI:10.1016/S0010-2180(01)00249-8

314 [5] T. A. Semelsberger, R. L. Borup, H. L. Greene. Dimethyl ether (DME) as an alternative fuel. *J. Power*  
315 *Sources* 156 (2006): 497-511. DOI:10.1016/j.jpowsour.2005.05.082

316 [6] R. Chen, H. Wang, H. Wang. Different oxygen levels of dimethyl ether combustion influence  
317 numerical simulation. *Procedia Engineering* 31 (2012): 934-940. DOI:10.1016/j.proeng.2012.01.1124

318 [7] S. H. Park, S. H. Yoon, J. Cha, C. S. Lee. Mixing effects of biogas and dimethyl ether (DME) on  
319 combustion and emission characteristics of DME fueled high-speed diesel engine. *Energy* 66 (2014):  
320 413-422. DOI:10.1016/j.energy.2014.02.007

321 [8] S. H. Yoon, J. P. Cha, C. S. Lee. An investigation of the effects of spray angle and injection strategy  
322 on dimethyl ether (DME) combustion and exhaust emission characteristics in a common-rail diesel  
323 engine. *Fuel Process. Technol.* 91 (2010): 1364-1372. DOI:10.1016/j.fuproc.2010.04.017

324 [9] I. M. Youn, S. H. Park, H. G. Roh, C. S. Lee. Investigation on the fuel spray and emission reduction  
325 characteristics for dimethyl ether (DME) fueled multi-cylinder diesel engine with common-rail injection  
326 system. *Fuel Process. Technol.* 92 (2011): 1280-1287. DOI:10.1016/j.fuproc.2011.01.018

327 [10] S. Bhattacharya, K. B. Kabir, K. Hein. Dimethyl ether synthesis from Victorian brown coal through  
328 gasification – Current status, and research and development needs. *Prog. Energ. Combust.* 39 (2013):  
329 577-605. DOI:10.1016/j.pecs.2013.06.003

330 [11] C. Arcoumanis, C. Bae, R. Crookes, E. Kinoshita. The potential of di-methyl ether (DME) as an  
331 alternative fuel for compression-ignition engines: A review. *Fuel* 87 (2008): 1014-1030.  
332 DOI:10.1016/j.fuel.2007.06.007

333 [12] S. Kajitani, Z. Chen, M. Oguma. A study of low-compression-ratio dimethyl ether diesel engines. *Int.*  
334 *J. Engine Res.* 3 (2002): 1-11. DOI:10.1243/1468087021545496

335 [13] G. Mittal, M. Chaos, C. Sung, F. L. Dryer. Dimethyl ether auto-ignition in a rapid compression  
336 machine: Experiments and chemical kinetic modeling. *Fuel Process. Technol.* 89 (2008): 1244-1254.  
337 DOI:10.1016/j.fuproc.2008.05.021

338 [14] Z. W. Zhao, M. Chaos, A. Kazakov, F. L. Dryer. Thermal decomposition reaction and a  
339 comprehensive kinetic model of dimethyl ether. *Int. J. Chem. Kinet.* 40 (2008): 1-18.  
340 DOI:10.1002/kin.20285

341 [15] Z. Zhao, A. Kazakov, F. L. Dryer. Measurements of dimethyl ether/air mixture burning velocities by  
342 using particle image velocimetry. *Combust. Flame* 139 (2004): 52-60.  
343 DOI:10.1016/j.combustflame.2004.06.009

344 [16] E. Kaiser, T. Wallington, M. Hurley, J. Platz, H. Curran, W. Pitz, C. K. Westbrook. Experimental and  
345 modeling study of premixed atmospheric-pressure dimethyl ether-air flames. *J. Phys. Chem. A* 35 (2000):  
346 8194-8206. DOI:10.1021/jp994074c

347 [17] Z. H. Huang, Q. Wang, J. R. Yu, Y. Zhang, K. Zeng, H. Y. Miao, D. M. Jiang. Measurement of  
348 laminar burning velocity of dimethyl ether-air premixed mixtures. *Fuel* 86 (2007): 2360-2366.  
349 DOI:10.1016/j.fuel.2007.01.021

350 [18] P. Dagaut, J. Boettner, M. Cathonnet. Chemical kinetic study of dimethyl ether oxidation in a jet  
351 stirred reactor from 1 to 10 atm: Experiments and kinetic modeling. *Proc. Combust. Inst.* 26 (1996):  
352 627-632. DOI:10.1016/S0082-0784(96)80269-4

353 [19] P. Dagaut, C. Daly, J. M. Simmie, M. Cathonnet. The oxidation and ignition of dimethyl ether from  
354 low to high temperature (500–1600 K): Experiments and kinetic modeling. *Proc. Combust. Inst.* 27  
355 (1998): 361-369. DOI:10.1016/S0082-0784(98)80424-4

356 [20] U. Burke, K. P. Somers, P. O'Toole, C. M. Zinner, N. Marquet, G. Bourque, E. L. Petersen, W. K.  
357 Metcalfe, Z. Serinyel, H. J. Curran. An ignition delay and kinetic modeling study of methane, dimethyl  
358 ether, and their mixtures at high pressures. *Combust. Flame* 162(2) (2015): 315-330.  
359 DOI:10.1016/j.combustflame.2014.08.014

360 [21] Z. Chen, X. Qin, Y. Ju, Z. Zhao, M. Chaos, F. L. Dryer. High temperature ignition and combustion  
361 enhancement by dimethyl ether addition to methane-air mixtures. *Proc. Combust. Inst.* 31 (2007):  
362 1215-1222. DOI:10.1016/j.proci.2006.07.177

363 [22] P. Dai, Z. Chen, S. Y. Chen. Ignition of methane with hydrogen and dimethyl ether addition. *Fuel*  
364 118 (2014): 1-8. DOI:10.1016/j.fuel.2013.10.048

365 [23] H. D. Ng, J. Chao, T. Yatsufusa, J. H. S. Lee. Measurement and chemical kinetic prediction of  
366 detonation sensitivity and cellular structure characteristics in dimethyl ether–oxygen mixtures. *Fuel* 88  
367 (2009): 124-131. DOI:10.1016/j.fuel.2008.07.029

368 [24] P. Diakow, M. Cross, G. Ciccarelli. Detonation characteristics of dimethyl ether and ethanol-air  
369 mixtures. *Shock Waves* 25 (3) (2015): 231-238. DOI:10.1007/s00193-015-0554-7

370 [25] T. Mogi, S. Horiguchi. Explosion and detonation characteristics of dimethyl ether. *J. Hazard. Mater.*  
371 164 (2009): 114-119. DOI:10.1016/j.jhazmat.2008.07.133

372 [26] T. Mogi, H. Shiina, Y. Wada, R. Dobashi. Investigation of the properties of the accidental release  
373 and explosion of liquefied dimethyl ether at a filling station. *J. Loss Prevent. Proc.* 26 (2013): 32-37.  
374 DOI:10.1016/j.jlp.2012.09.002

375 [27] A. A. Konnov. The temperature and pressure dependences of the laminar burning velocity:  
376 experiments and modeling. Proc. 7<sup>th</sup> European Combustion Meeting, Budapest, Hungary, March 30-April  
377 2, (2015).

378 [28] C. K. Law (2006). *Combustion Physics*, Cambridge University Press, New York.

379 [29] B. Zhang, G. L. Xiu, C. H. Bai. Explosion characteristics of argon/nitrogen diluted natural gas-air  
380 mixtures. *Fuel* 124 (2014): 125-132. DOI:10.1016/j.fuel.2014.01.090

381 [30] R. J. Kee, J. F. Grcar, M. D. Smooke, J. A. Miller. A Fortran Program for Modeling Steady Laminar  
382 One-Dimensional Premixed Flames. Report No. SAND85-8240, 1985

383 [31] A. E. Dahoe, J. F. Zevenbergen, S. M. Lemkowitz, B. Scarlett. Dust explosions in spherical vessels:  
384 the role of flame thickness in the validity of the 'cube-root law'. *J. Loss Prevent. Proc.* 9 (1996): 33-44.  
385 DOI:10.1016/0950-4230(95)00054-2

386 [32] A. E. Dahoe. Laminar burning velocities of hydrogen-air mixtures from closed vessel gas explosions.  
387 *J. Loss Prevent. Proc.* 18 (2005): 152-166. DOI:10.1016/j.jlp.2005.03.007

388 [33] X. Qin, Y. Ju. Measurements of burning velocities of dimethyl ether and air premixed flames at  
389 elevated pressures. *Proc. Combust. Inst.* 30 (2005): 233-240. DOI:10.1016/j.proci.2004.08.251

390 [34] B. Zhang, C. H. Bai. Critical energy of direct detonation initiation in gaseous fuel-oxygen mixtures.  
391 *Safety Sci.* 53 (2013): 153-159. DOI:10.1016/j.ssci.2012.09.013

392 [35] B. Zhang, C. H. Bai, G. L. Xiu, Q. M. Liu, G. D. Gong. Explosion and flame characteristics of  
393 methane/air mixtures in a large-scale vessel. *Process Saf. Prog.* 33 (2014):  
394 362-368. DOI:10.1002/prs.11670

395 [36] B. Zhang, V. Kamenskihs, H. D. Ng, J. H. S. Lee. Direct blast initiation of spherical gaseous  
396 detonations in highly argon diluted mixtures. *Proc. Combust. Inst.* 33 (2011): 2265-2271.  
397 DOI:10.1016/j.proci.2010.06.165

- 398 [37] B. Zhang, N. Mehrjoo, H. D. Ng, J. H. S. Lee, C. H. Bai. On the dynamic detonation parameters in  
399 acetylene-oxygen mixtures with varying amount of argon dilution. *Combust. Flame* 161 (2014):  
400 1390-1397. DOI:10.1016/j.combustflame.2013.11.016
- 401 [38] B. Zhang, H. D. Ng, J. H. S. Lee. The critical tube diameter and critical energy for direct initiation  
402 of detonation in  $C_2H_2/N_2O/Ar$  mixtures. *Combust. Flame* 159 (2012): 2944-2953.  
403 DOI:10.1016/j.combustflame.2012.06.010
- 404 [39] B. Zhang, H. D. Ng, R. Mével, J. H. S. Lee. Critical energy for direct initiation of spherical  
405 detonations in  $H_2/N_2O/Ar$  mixtures. *Int. J. Hydrogen Energ.* 36 (2011): 5707-5716.  
406 DOI:10.1016/j.ijhydene.2011.01.175
- 407 [40] M. Hattwig, G. Steen (2004). *Handbook of Explosion Prevention and Protection*, Wiley-VCH,  
408 Weinheim.
- 409 [41] B. S. Nie, X. Q. He, R. M. Zhang, W. X. Chen, J. F. Zhang. The roles of foam ceramics in  
410 suppression of gas explosion overpressure and quenching of flame propagation. *J. Hazard. Mater.* 192  
411 (2011): 741-747. DOI:10.1016/j.jhazmat.2011.05.083
- 412 [42] B. S. Nie, H. Q. He, C. Zhang, X. C. Li, H. L. Li. Temperature measurement of gas explosion flame  
413 based on the radiation thermometry. *Int. J. Therm. Sci.* 78 (2014): 132-44.  
414 DOI:10.1016/j.ijthermalsci.2013.12.010
- 415 [43] C. Wang, X. Dong, J. Ding, B. Nie. Numerical investigation on the spraying and explosibility  
416 characteristics of coal dust. *Int. J. Mining Reclamation and Environment* 28 (2014): 287-296.  
417 DOI:10.1080/17480930.2014.964041
- 418 [44] Z. Wang, M. Pan, S. Wang, D. Sun. Effects on external pressures caused by vented explosion of  
419 methane-air mixtures in single and connected vessels. *Process Saf. Prog.* 33 (2014): 385-391.  
420 DOI:10.1002/prs.11668
- 421 [45] Z. R. Wang, M. Y. Pan, J. C. Jiang. Experimental investigation of gas explosion in single vessel and  
422 connected vessels. *J. Loss Prevent. Proc.* 26 (2013): 1094-1099. DOI:10.1016/j.jlp.2013.04.007
- 423 [46] Z. R. Wang, L. Ni, X. Liu, J. C. Jiang, R. Wang. Effects of  $N_2/CO_2$  on explosion characteristics of  
424 methane and air mixture. *J. Loss Prevent. Proc.* 31 (2014): 10-15. DOI:10.1016/j.jlp.2014.06.004
- 425 [47] GASEQ. A Chemical Equilibrium Program for Windows. Available from:  
426 <http://www.c.morley.dsl.pipex.com/>
- 427 [48] M. Kuzetsov J. Grune, T. Jordan. Flammability limits and laminar flame speed of hydrogen-air

428 mixtures at sub-atmospheric pressures. *Int. J. hydrogen Energy* 37 (22) (2012): 17580-17588.  
429 DOI:10.1016/j.ijhydene.2012.05.049

430 [49] Q. Z. Li, B. Q. Lin, H. M. Dai, S. Zhao. Explosion characteristics of H<sub>2</sub>/CH<sub>4</sub>/air and CH<sub>4</sub>/coal  
431 dust/air mixtures. *Powder Technol.* 229 (2012): 222-228. DOI:10.1016/j.powtec.2012.06.036

432 [50] Y. D. Jo, D. A. Crowl. Explosion characteristics of hydrogen-air mixtures in a spherical vessel.  
433 *Process Saf. Prog.* 29 (2009): 216-223. DOI:10.1002/prs.10370

434 [51] A. Di Benedetto, V. Di Sarli, E. Salzano, F. Cammarota, G. Russo. Explosion behavior of  
435 CH<sub>4</sub>/O<sub>2</sub>/N<sub>2</sub>/CO<sub>2</sub> and H<sub>2</sub>/O<sub>2</sub>/N<sub>2</sub>/CO<sub>2</sub> mixtures. *Int. J. Hydrogen Energ.* 34 (2009): 6970-6978.  
436 DOI:10.1016/j.ijhydene.2009.05.120

437 [52] M. Kuznetsov, R. Redlinger, W. Breitung, J. Grune, A. Friedrich, N. Ichikawa. Laminar burning  
438 velocities of hydrogen-oxygen-steam mixtures at elevated temperatures and pressures. *Proc. Combust.*  
439 *Inst.* 33 (2011): 895-903. DOI:10.1016/j.proci.2010.06.050

440 [53] S. K. Paidi, A. Bhavaraju, M. Akram, S. Kumar. Effect of N<sub>2</sub>/CO<sub>2</sub> dilution on laminar burning  
441 velocity of H<sub>2</sub>-air mixtures at high temperatures. *Int. J. Hydrogen Energ.* 38 (2013): 13812-13821.  
442 DOI:10.1016/j.ijhydene.2013.08.024

443 [54] C. Prathap, A. Ray, M. R. Ravi. Investigation of nitrogen dilution effects on the laminar burning  
444 velocity and flame stability of syngas fuel at atmospheric condition. *Combust. Flame* 155 (2008):  
445 145-160. DOI:10.1016/j.combustflame.2008.04.005

446 [55] B. Zhang, H. D. Ng. Explosion behavior of methane-dimethyl ether/air mixtures. *Fuel* 157 (2015):  
447 56-63. DOI:10.1016/j.fuel.2015.04.058

448 [56] K. Takizawa, A. Takahashi, K. Tokuhashi, S. Kondo, A. Sekiya. Burning velocity measurement of  
449 fluorinated compounds by the spherical-vessel method. *Combust. Flame* 141 (2005): 298-307.  
450 DOI:10.1016/j.combustflame.2005.01.009

451 [57] E. Salzano, F. Cammarota, A. Di Benedetto, V. Di Sarli. Explosion behavior of  
452 hydrogen-methane/air mixtures. *J. Loss Prevent. Proc.* 25(3) (2012): 443-447.  
453 DOI:10.1016/j.jlp.2011.11.010

454 [58] Z. H. Huang, Y. Zhang, K. Zeng, B. Liu, Q. Wang, D. M. Jiang. Measurements of laminar burning  
455 velocities for natural gas-hydrogen-air mixtures. *Combust. Flame* 146 (2006): 302-311.  
456 DOI:10.1016/j.combustflame.2006.03.003

457  
458

459

460 **Tables**

461

462 Table. 1 Mixture compositions for the experimental tests, along with maximum explosion

463 pressure  $p_{\max}$ , corresponding combustion time  $t_c$ , and adiabatic pressure  $p_{\text{ad}}$

464 Table. 2 Flammability limits of DME-air at different initial pressures

465

466

467  
468  
469  
470  
471

Table. 1

Test n.	DME % v/v	O <sub>2</sub> % v/v	N <sub>2</sub> % v/v	$p_{ad}$ MPa	$p_{max}$ MPa	$p_{ad}-p_{max}$ MPa	$t_c$ s
1	3.0	20.37	76.63	0.6042	0.1000	0.5042	—
2	3.5	20.27	76.24	0.6699	0.1446	0.5253	0.3574
3	4.0	20.16	75.84	0.7316	0.4687	0.2629	0.2612
4	5.0	19.95	75.05	0.8406	0.8844	-0.0438	0.1064
5	6.0	19.74	74.26	0.9244	1.0011	-0.0767	0.0726
6	6.5	19.64	73.87	0.9548	1.0578	-0.1030	0.0732
7	7.0	19.53	73.47	0.9770	1.0767	-0.0997	0.0610
8	7.5	19.43	73.08	0.9908	1.0781	-0.0873	0.0668
9	8.0	19.32	72.68	0.9971	1.0447	-0.0476	0.0610
10	9.0	19.11	71.89	0.9953	0.9953	0.0000	0.0736
11	10.0	18.90	71.10	0.9847	0.9157	0.0690	0.1042
12	11.0	18.69	70.31	0.9704	0.7448	0.2256	0.1752
13	12.0	18.48	69.52	0.9540	0.5341	0.4199	0.2888
14	13.0	18.27	68.73	0.9358	0.3364	0.5994	0.3867
15	14.0	18.06	67.94	0.9161	0.2532	0.6629	1.0900
16	15.0	17.85	67.15	0.8949	0.1810	0.7139	1.2050
17	16.0	17.64	66.36	0.8724	0.1286	0.7438	1.3134
18	17.0	17.43	65.57	0.8486	0.1218	0.7268	1.3265
19	18.0	17.22	64.78	0.8236	0.1195	0.7041	1.4118
20	19.0	17.01	63.99	0.7972	0.1192	0.6780	1.4339
21	19.5	16.91	63.60	0.7836	0.1000	0.6836	—

472  
473

474  
475  
476  
477  
478  
479  
480  
481

Table. 2

$p_0$ (kPa)	LFL (% v/v)	UFL (% v/v)
100	3.50	19.00
80	3.75	15.00
60	3.33	14.17
40	3.75	12.50

482  
483

484

485 **Figure captions**

486 Fig. 1 The 20-L explosion spherical vessel (1 = DME, 2 = air).

487 Fig. 2 Determination of the maximum explosion pressure and the combustion time from a  
488 typical experimental pressure history.

489 Fig. 3  $p_{\max}$  as a function of DME concentration, compared with Mogi and Horiguchi [25]  
490 and adiabatic pressure from equilibrium calculations ( $p_0 = 100$  kPa). A curve fit of  $p_{\max}$   
491 is also shown in the plot.

492 Fig. 4  $p_{\max}$  as a function of DME concentration, compared with chemical adiabatic pressure  
493 from equilibrium calculations at an initial pressure of  $p_0 = 80$  kPa. A curve fit of  $p_{\max}$  is  
494 also shown in the plot.

495 Fig. 5  $p_{\max}$  as a function of DME concentration, compared with adiabatic pressure from  
496 equilibrium calculations at an initial pressure of  $p_0 = 60$  kPa. A curve fit of  $p_{\max}$  is also  
497 shown in the plot.

498 Fig. 6  $p_{\max}$  as a function of DME concentration, compared with adiabatic pressure from  
499 equilibrium calculations at an initial pressure of  $p_0 = 40$  kPa. A curve fit of  $p_{\max}$  is also  
500 shown in the plot.

501 Fig. 7 Maximum rate of pressure rise as a function of DME concentration for different initial  
502 pressures. Curve fits (shown by the solid lines) are also provided to show the trend in  
503 the data.

504 Fig. 8 Comparison of the laminar burning velocity from chemical simulation and experiment  
505 at an initial pressure of  $p_0 = 100$  kPa, Data from Qin and Ju [33] and Daly et al. [4] are  
506 also shown for comparison.

507 Fig. 9 Comparison of the laminar burning velocity calculated by detailed reaction kinetic  
508 simulations and determined from explosion properties: (a) 80 kPa, (b) 60 kPa; and (c)  
509 40 kPa.

510 Fig. 10 Dimensionless radius of burned DME-air mixtures with an equivalent ratio of  $\varphi = 1$  at  
511 different initial pressures.

512

513

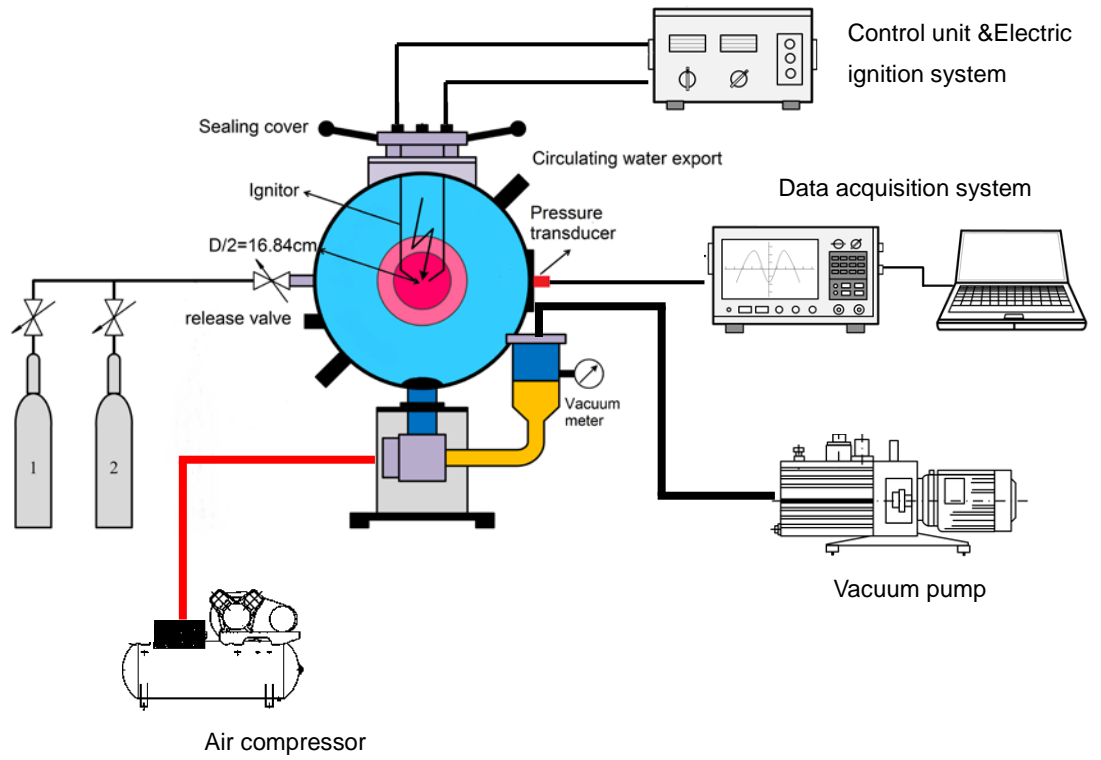
514

515

516

517

518



519

520

521

522

523

524

525

526

527

528

Fig.1

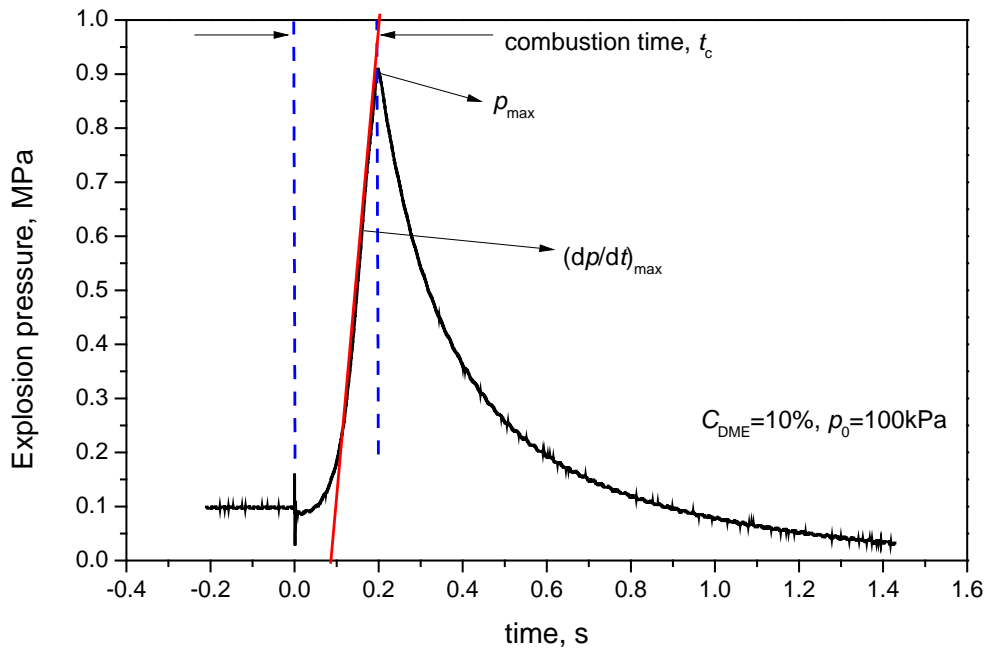
529

530

531

532

533



534

535

536

Fig.2

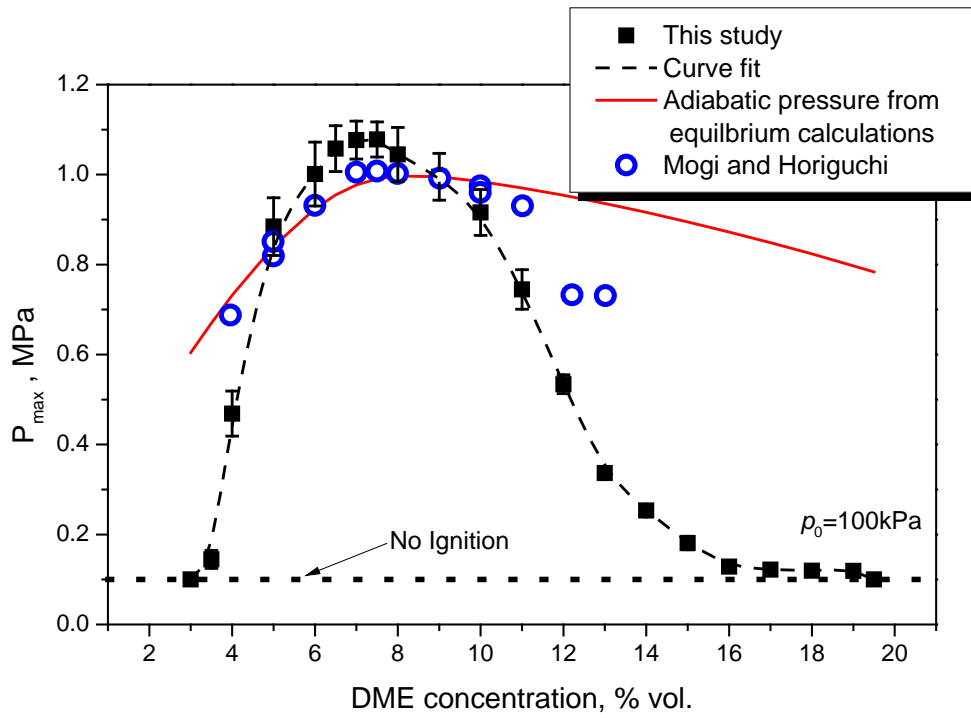
537

538

539

540

541



542

543

544

Fig.3

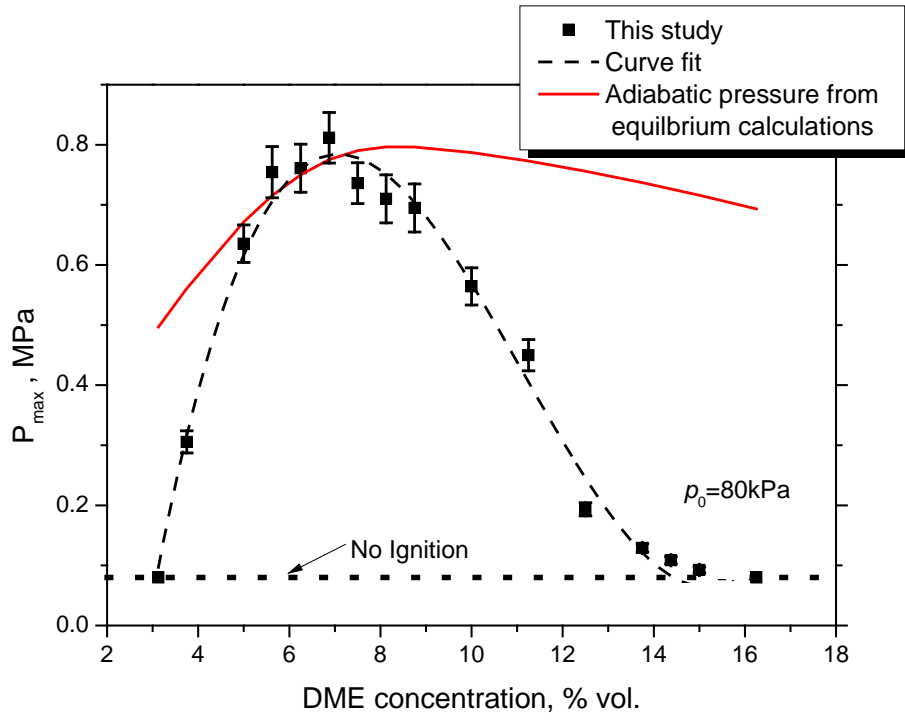
545

546

547

548

549



550

551

552

Fig.4

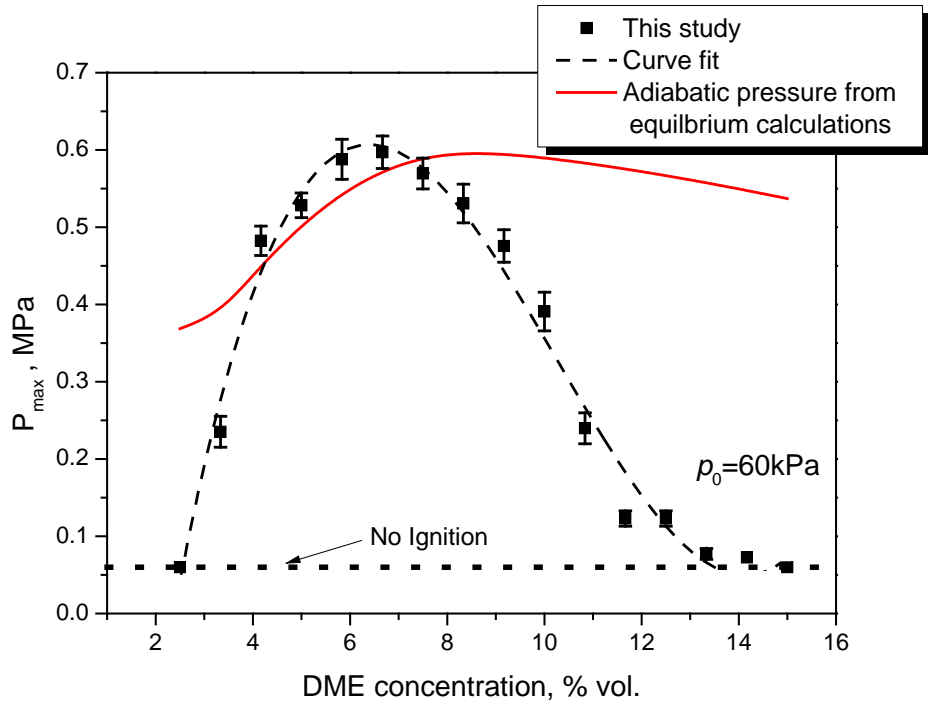
553

554

555

556

557



558

559

560

Fig.5

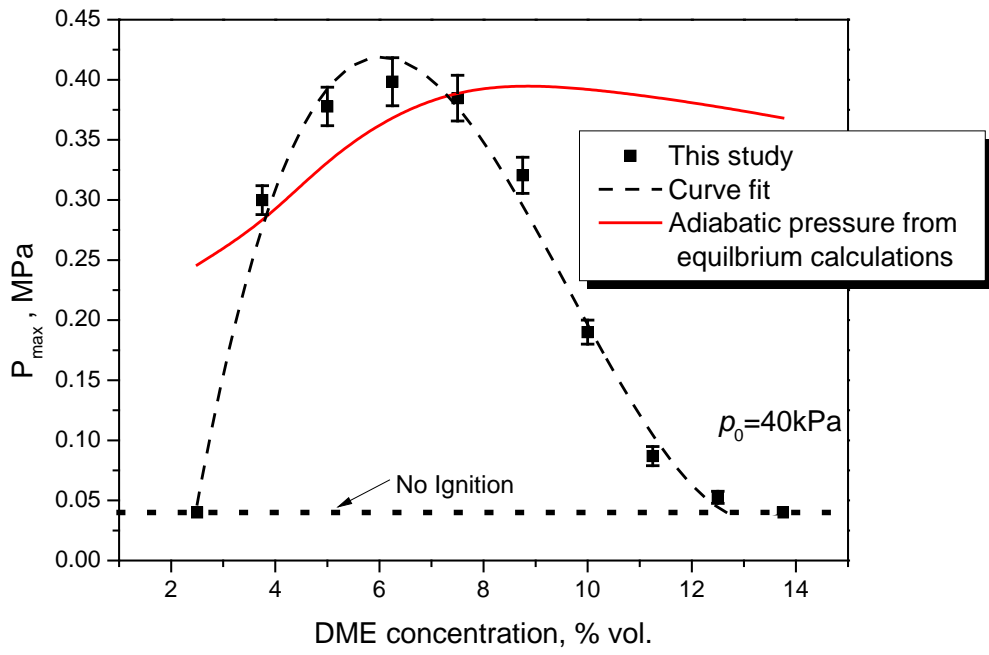
561

562

563

564

565



566

567

568

Fig.6

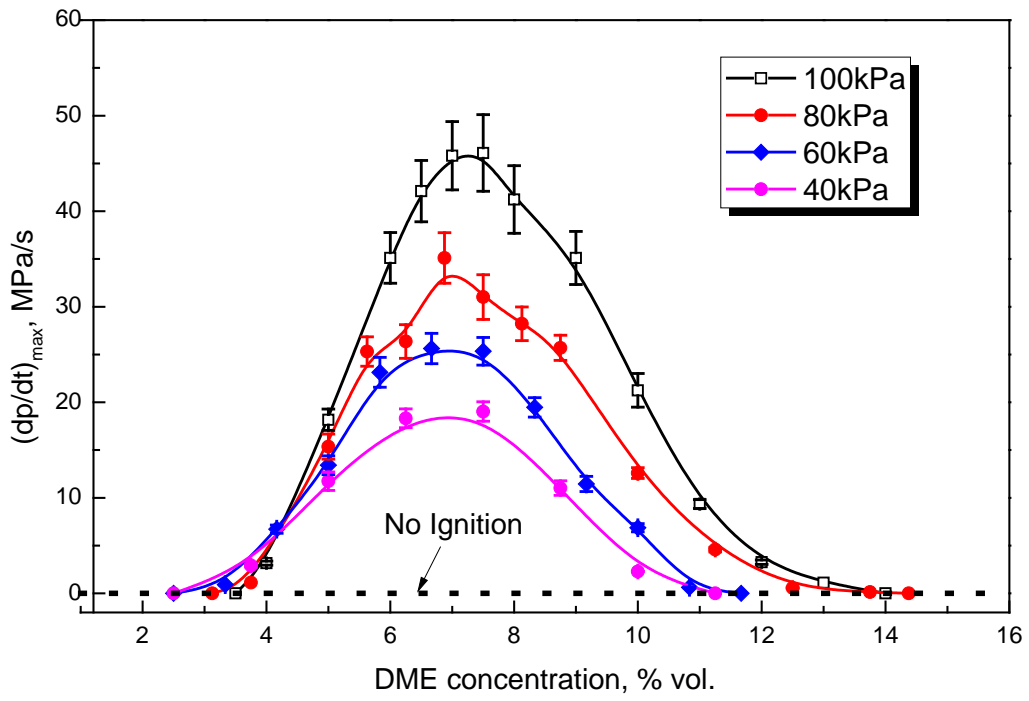
569

570

571

572

573



574

575

576

Fig.7

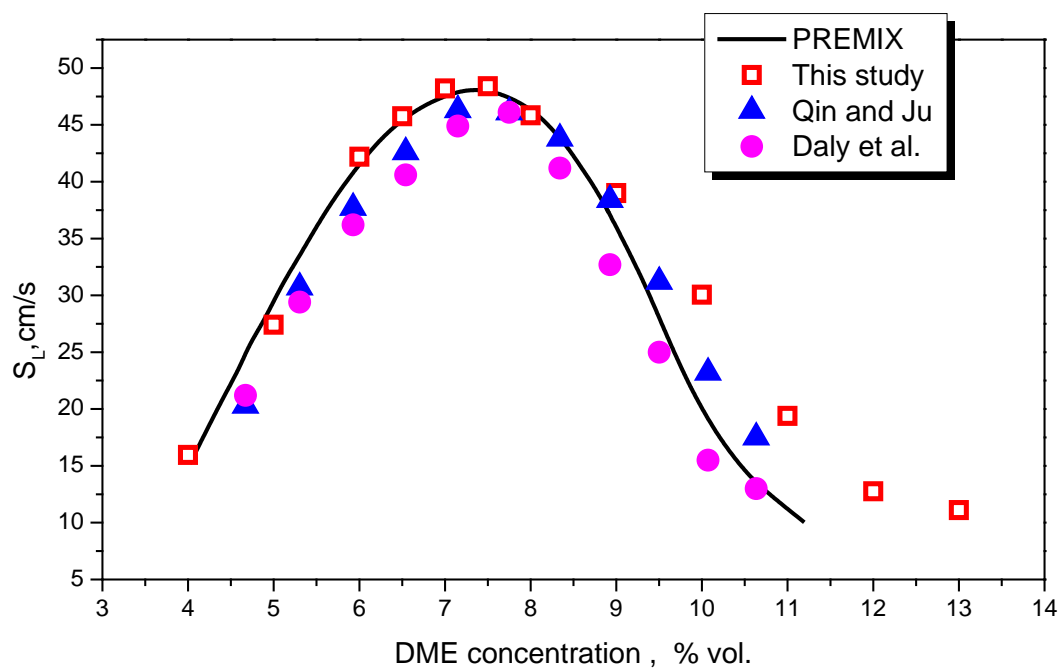
577

578

579

580

581



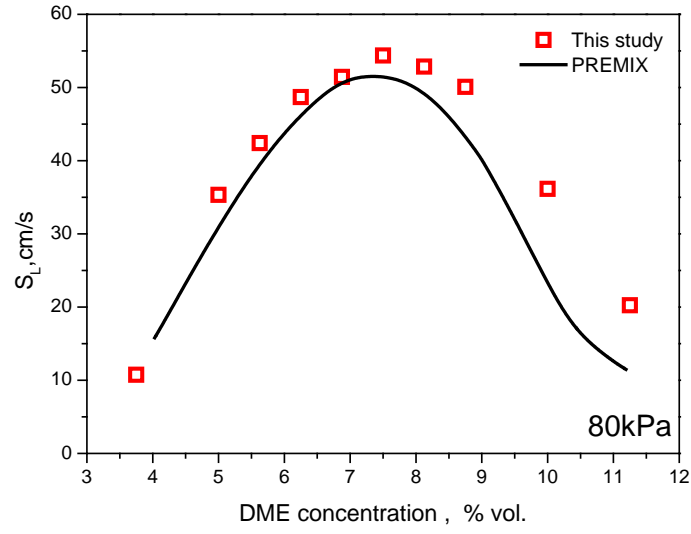
582

583

584

Fig. 8

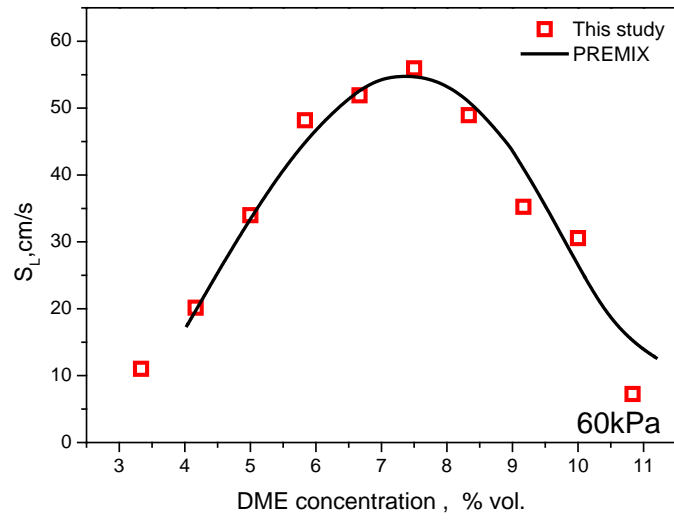
585



586

587

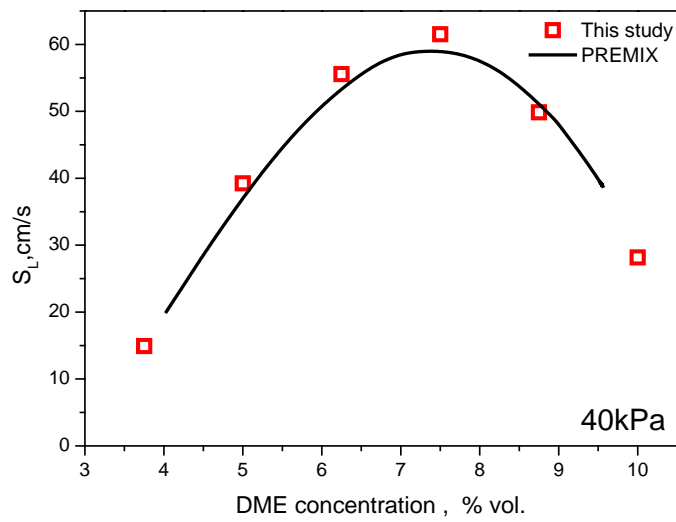
(a)



588

589

(b)



590

591

592

(c)

Fig.9

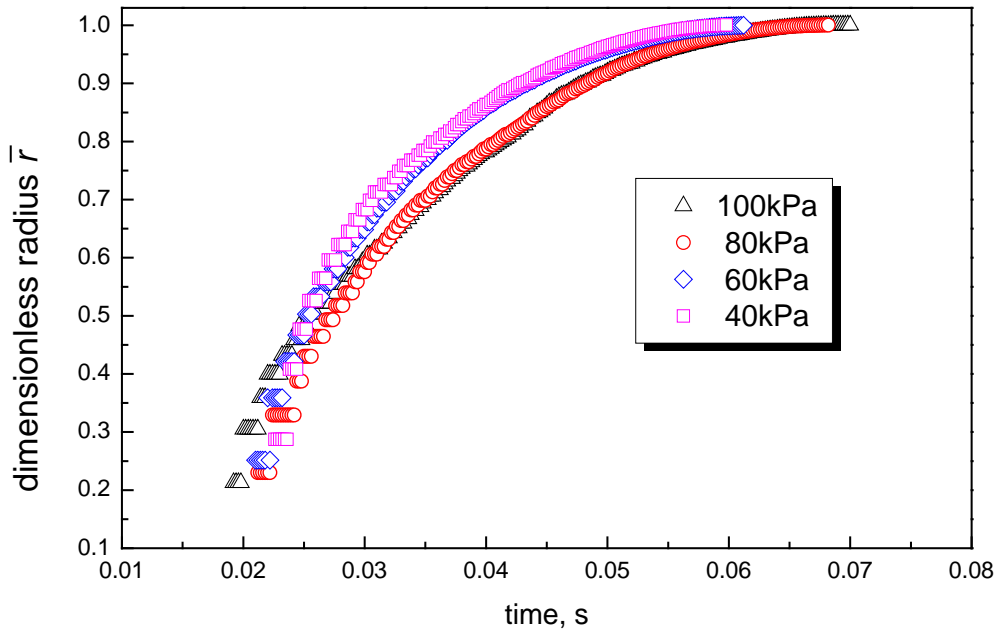
593

594

595

596

597



598

599

600

Fig.10